International Journal of Nanomedicine

Dovepress
Taylor & Francis Group

Open Access Full Text Article

ORIGINAL RESEARCH

Synergistic Enhancement of Therapeutic Efficacy in Acute Myocardial Infarction via Nanoflower-Like Mn_3O_4 Nanozymes in Coordination with Adipose-Derived Stem Cell Transplantation

Rui Gao[1,*], Demeng Xia[2,*], Xiaoyong Zhang[3,*], Yao Xiao[3], Hong Zhou[3], Gan Chen[3], Haibin Wang[1]

[1]College of Life Science and Bioengineering, College of Physical Science and Engineering, Beijing Jiaotong University, Beijing, 100044, People's Republic of China; [2]Department of Orthopaedics, Shanghai General Hospital, Shanghai Jiao Tong University School of Medicine, Shanghai, 200000, People's Republic of China; [3]Institute of Health Service and Transfusion Medicine, Academy of Military Medical Sciences, Beijing, 100850, People's Republic of China

*These authors contributed equally to this work

Correspondence: Gan Chen, Email chenlzu2005@163.com; Haibin Wang, Email wanghb@bjtu.edu.cn

Background: Acute myocardial infarction (AMI) is a leading cause of mortality worldwide. Adipose-derived stem cell (ADSC) transplantation presents a promising therapeutic approach for AMI; however, the harsh microenvironment of the infarcted myocardium, characterized by hypoxia and oxidative stress, limits the survival and efficacy of ADSCs. Nanozymes (NZs), which have robust anti-oxidative enzyme-mimicking activities, have demonstrated potential in combating oxidative stress and improving cell viability.

Methods: Mn3O4 NZs (Mn-Nzs), which have nanoflower-like structures were synthesized and their structure and multi-enzyme mimetic activities (superoxide dismutase, catalase, and glutathione peroxidase) were characterized. Blood biochemical parameters were measured in the heart, liver, spleen, lungs and kidneys of the rats, followed by hematoxylin and eosin (HE) staining. The impact of Mn3O4 NZs on reactive oxygen species (ROS) levels, and viability of ADSCs under oxidative stress was assessed in vitro. In vivo studies were conducted using a rat AMI model to evaluate the therapeutic efficacy of ADSC transplantation, in conjunction with Mn3O4 treatment. In addition, proteomic analysis was performed to elucidate the mechanisms of action underlying the therapeutic effects.

Results: Mn_3O_4 NZs exhibited multi-enzyme mimetic activities, including superoxide dismutase, catalase, and glutathione peroxidase, reducing reactive oxygen species levels and apoptosis in ADSCs under oxidative stress. In the AMI rat model, Mn-NZs had good biocompatibility and ADSC transplantation or Mn_3O_4 NZs treatment alone significantly reduced infarct size, fibrosis levels, and improved microvascular density and heart function. Notably, the combination of Mn_3O_4 NZs with ADSC transplantation enhanced ADSC survival and differentiation, amplifying therapeutic efficacy. Proteomic analysis revealed that Mn_3O_44 NZs upregulated proteins associated with anti-oxidative damage, anti-inflammation, and anti-fibrosis pathways. In addition, Mn-NZs upregulated MMP8 via AKT pathway phosphorylation.

Conclusion: The findings highlight a novel strategy integrating NZ anti-oxidant properties with stem cell transplantation to improve AMI treatment outcomes.

Keywords: acute myocardial infarction, adipose-derived stem cell, nanozymes, Mn_3O_4

Received: 23 June 2024
Accepted: 11 February 2025
Published: 17 February 2025

Introduction

Acute myocardial infarction (AMI) remains the leading cause of death in humans and imposes a tremendous economic burden on global health. AMI is a major contributor to cardiac remodeling, and heart failure remains the leading cause of morbidity and mortality worldwide.[1] The reopening of blocked vessels is a crucial part of AMI therapy to prevent further ischemic damage to the myocardium. However, reperfusion of the ischemic myocardium alone can result in reperfusion damage, which can increase infarct size by up to 50%.[2] Other existing treatment methods relieve the symptoms of patients to a certain extent, but fundamentally, they do not solve the problem of myocardial cell death and myocardial tissue damage after ischemia, which will eventually lead to heart failure.

With an increase in cardiovascular research, stem cell transplantation strategies have been developed to repair damaged heart tissue and improve heart function.[3,4] At present, many types of stem cells have been used in the treatment of AMI in basic research and clinical trials, which have proven the effectiveness and safety of stem cell transplantation.[5,6] Mesenchymal stromal/stem cells (MSCs) have been explored as a viable therapeutic strategy for AMI because of their biological characteristics. Compared with bone marrow MSCs, adipose-derived stem cells (ADSCs) are more readily and abundantly collected using minimally invasive techniques. In recent years, ADSC transplantation has been proven to be an effective treatment for AMI and the multi-differentiation potential of ADSCs, including their ability to differentiate into cardiomyocytes, vascular endothelial cells, and vascular smooth muscle cells, has been demonstrated.[7] Besides, ADSCs can also accelerate cell proliferation, anti-inflammation, and angiogenesis by secreting paracrine factors. For instance, the ADSCs produced cytokines such as vascular endothelial growth factor (VEGF), which is essential for inducing capillaries.[8] In addition, ADSC-derived extracellular vesicles promote cardiac regeneration by ameliorating cardiac fibrosis in infarcted hearts.[9] Yoshizaki et al reported that ADSCs could promote recovery from the ischemic condition in vivo.[10] In terms of clinical translation, a Phase I clinical trial (ClinicalTrials.gov ID NCT04695522) has been conducted in patients with the coronary artery bypass grafting (CABG) and found that ADSC contributed to capillary network reconstruction and cardiac function enhancement.[11] Similar studies regarding myocardial infarction intervention have also been conducted in clinical trials, like: NCT01216995, NCT00442806, and NCT01974128. Mechanistically, ADSCs transplantation therapy presents considerable potential in cardiac recovery.

However, owing to the influence of adverse microenvironments such as hypoxia, ischemia, oxidative stress, and inflammation in the local myocardial tissue that are present during AMI, the resident and survival rates of stem cells directly delivered to the infarcted myocardium are insufficient, and normal biological function is difficult, which affects the repair effect. To improve the adverse microenvironment of AMI, functional biomaterials, growth factors, and drugs can be delivered into the infarcted myocardium with stem cells, and the survival and biological function of stem cells can be ameliorated by regulating the microenvironment of AMI tissue. Although these strategies have improved treatment effectiveness, their overall effectiveness still needs to be further improved to meet treatment needs.

Nanozymes (NZs), which are nanomaterials with enzymatic properties, have attracted much attention for their potential applications in biomedicine.[12] Compared to natural proteases, NZs have higher catalytic stability, are easy to modify, and have lower manufacturing costs. In addition, many metal nanoparticles exhibit excellent anti-oxidative enzyme-mimicking activity, including superoxide dismutase (SOD), catalase (CAT), and glutathione peroxidase (GPx). Among them, Mn_3O_4 nanozymes (Mn_3O_4 NZs) have been shown to have anti-oxidative abilities, thus improving cell viability[13] and exerting therapeutic effects in oxidative stress-related diseases, including Parkinson's disease and Alzheimer's disease.[14–16] However, the therapeutic effects of Mn_3O_4 NZs alone and in conjunction with stem cell transplantation on AMI have not yet been realized.[17]

Therefore, in this study, we aimed to determine the efficiency of ADSCs transplantation combined with nanoflower-like Mn_3O_4 NZs in treating AMI and explore the underlying therapeutic mechanisms of action (Scheme 1).

Materials and Methods

Synthesis of Mn_3O_4 NZs

Mn_3O_4 NZs were synthesized following an existing standard procedure with some modifications.[15] Briefly, 2.0 g of $KMnO_4$ (Sinopharm Chemical Reagent, Shanghai, China) was dissolved in 1000 mL of ddH_2O under magnetic stirring for 30 min, and 20 mL of oleic acid (Sigma, St Louis, MO, USA) was added to the reaction mixture. After stirring for

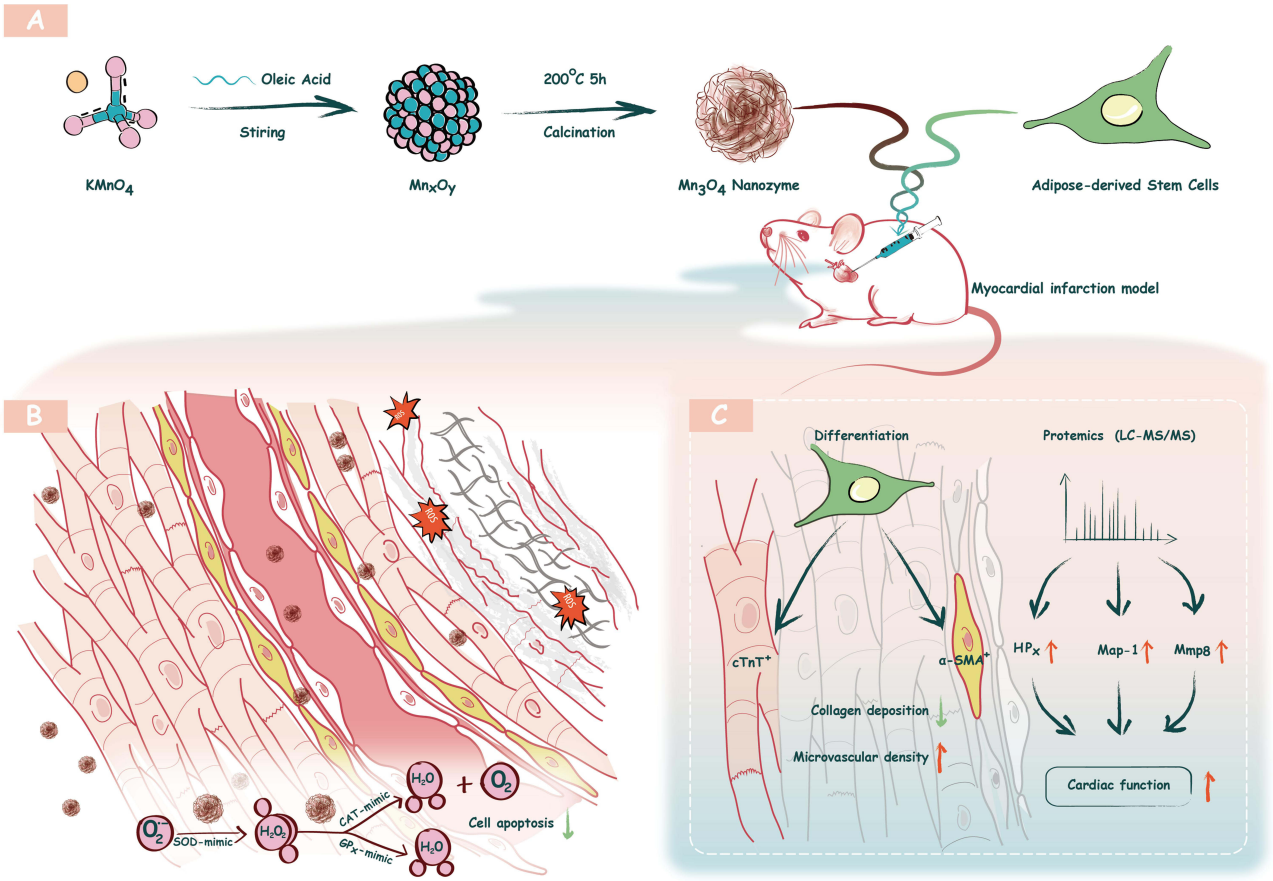

Scheme 1 Schematic illustration of the fabrication procedure of Mn_3O_4 NZs and the underlying therapeutic mechanism of Mn_3O_4 NZs against acute myocardial infarction injury. (**A**) $KMnO_4$ is dissolved into ddH_2O, then oleic acid is added into the reaction mixture. The precipitates are washed with ddH_2O and ethanol, and then the product is further calcined at 200°C in air to obtain Mn_3O_4 NZs. (**B**) Mn_3O_4 NZs improve the MI microenvironment area through anti-oxidative pathway. (**C**) Mn_3O_4 NZs + ADSCs improves the survival and differentiation of ADSCs after transplantation in AMI rats.
Abbreviations: NZs, nanozymes; ADSC, adipose-derived stem cell; AMI, acute myocardial infarction.

5 h, the precipitates were washed with ddH_2O and ethanol, then dried (10 h, 80°C) to obtain precursor particles, and the precursor was further calcined at 200°C for 5 h in air to obtain Mn_3O_4 NZs.

Characterization of Mn_3O_4 NZs

The morphology of Mn_3O_4 NZs was characterized using transmission electron microscopy (TEM; ULVAC-PHI). The elemental valence states and chemical composition of Mn_3O_4 NZs were analyzed using X-ray photoelectron spectroscopy (XPS). The chemical structure of Mn_3O_4 NZs was examined using Fourier-transform infrared spectroscopy (FTIR; Thermo Fisher Scientific Nicolet iS20) and Raman spectroscopy (Raman; Horiba LabRAM HR Evolution). Full-wavelength Mn_3O_4 NZs scanning was performed using a microplate reader (SPECTROstar Omega).

Multi-Anti-Oxidative Enzyme Mimetic Activities of Mn_3O_4 NZs

The SOD- and CAT-mimetic activities of the Mn_3O_4 NZs were measured using SOD and CAT assay kits (Nanjing Jiancheng Bioengineering Institute, Nanjing, China), as previously described.[18,19]

The GPx-mimetic activity of the Mn_3O_4 NZs was evaluated using a GPx assay kit (Beyotime Biotechnology, Shanghai, China) according to the manufacturer's instructions.

https://doi.org/10.2147/IJN.S483980

Characterization of ADSCs

Flow Cytometry

ADSCs were digested with a 0.25% trypsin (SL6010, Coolaber, Beijing, China) solution at passage 3, and the detached cultured cells were washed several times with phosphate-buffered saline (PBS, 10010023, Gibco, Grand Island, NY, USA). The pellets were suspended, and the cells were counted. Notably, 1×10^6 cells/mL were suspended in α-MEM (12561056, Gibco) medium. Cells are then treated and incubated for 30 min at 4°C with fluorescently-labeled antibodies against CD31 (SC-71873, Santa Cruz Biotechnology Inc., Dallas, TX, USA), CD34 (SC-7324, Santa Cruz), CD90 (206105, Bio Legend, San Diego, CA, USA), CD45 (202205, Bio Legend), and CD29 (102205, Bio Legend). Cells were washed twice with PBS containing 3% FBS (A5670701, Gibco) and 300 μL 2% paraformaldehyde (SL1830, Coolaber) was added. The cells were then fixed and analyzed using FACSCalibur (BD Biosciences, San Diego, CA, USA).

Adipogenic Differentiation

ADSCs were cultured in adipogenic differentiation medium containing 10% FBS, 0.5 mm 3-isobutyl-methylxanthine (I793835, Macklin, Shanghai, China), 1 μM dexamethasone (D793754, Macklin), 10 μM insulin (I5523, Sigma, St Louis, MO, USA), 200 μM indomethacin (I797872, Macklin), and 1×penicillin-Streptomycin Solution (C0222, Beyotime Biotechnology), and α-MEM for two weeks. Intracellular lipids accumulation was detected using Oil Red O staining.[4,20]

Osteogenic Differentiation

ADSCs were cultured with osteogenic differentiation medium containing 0.01 μM dexamethasone, 50 μM ascorbate acid-2-phosphate (A4403, Sigma), 10 mm b-glycerophosphate (G9422, Sigma), 1×Penicillin-Streptomycin Solution, α-MEM, and 10% FBS for 2 weeks. Differentiation was defined by characterization under alkaline phosphatase staining at the end of two weeks.[20]

Rat AMI Model

Sprague–Dawley (SD) rats were anesthetized with an intraperitoneal injection of pentobarbital sodium (30 mg/kg) and artificially ventilated using a small animal ventilator (DW-3000, Pushin) with a tidal volume of 6 mL at a rate of 80 cycles/min. Left thoracotomy was performed between the 3rd and the 4th ribs to expose the heart. The left anterior descending coronary artery was ligated directly under the origin, 2–3 mm from the left atrial appendage, using a 6–0 suture. Occlusion was confirmed by immediate pallor of the anterior wall of the left ventricle, regional hypokinesia, enlargement of the left ventricle, and closure of the thorax and skin. All procedures were performed under sterile conditions. Then, 100 μL of Mn3O4 NZs (20 mg/mL) or ADSCs with cell content of 5×106 were intramyocardially injected around the myocardial infarction (MI) region, and the control group was treated with 100 μL of PBS. All experimental procedures were approved by the Institutional Animal Ethics Committee of Beijing Jiao Tong University according to the Guide for the Care and Use of Laboratory Animals of the National Institutes of Health.

Pathological Staining

For histopathological analysis, heart samples were harvested 2 or 4 weeks after AMI. Tissues were sectioned at a thickness of 4 μm and stained with Masson trichrome staining and immunohistochemical staining to detect von Willebrand factor (vWF). Anti-Von Willebrand Factor antibody (ab6994) was purchased from Abcam (Cambridge, London, UK). Five fields in each slice were chosen for quantification. ImageJ software (NIH, Bethesda, MD, USA) was used to calculate the percentage of MI area and the percentage of collagen fibers that accounted for the total infarction area. The infarct area was calculated by measuring the endocardial and epicardial surface lengths delimiting the infarct region, as detected by Masson's trichrome staining. The ImageJ software (NIH) was used to calculate the percentage of collagen fibers that accounted for the total infarction area.

Mn_3O_4 NZs Pre-Treatment of ADSCs in an H_2O_2-Induced Oxidative Stress Model

ADSCs were cultured in 6-well plates at a density of 2×10^5 cells/well. ADSCs were pre-treated with different concentrations of Mn_3O_4 NZs for 3 h, the supernatant was discarded, and the cells were washed twice with PBS.

Then, 30 μM H_2O_2 was added to the culture medium to induce an oxidative stress model. One hour later, the intracellular reactive oxygen species (ROS) level was detected using a dihydroethidium (DHE, R001, Vigorous Biotechnology, Beijing, China) assay, and cell viability was measured by Live/Dead Viability Kits (1862142, Thermo Fisher, Waltham, MA, USA).

Echocardiographic Measurements

The cardiac function of mice subjected to AMI after 4 weeks was evaluated using echocardiography (ECG). The rats were anesthetized with pentobarbital sodium and placed in the supine position on an ultrasonic workstation that monitored ECG, respiratory rate, and pulse. After the heart rate was stabilized, transthoracic two-dimensional exercise mode ECG (VisualSonics Inc., Toronto, Canada) was performed. The Vevo1100 software program (VisualSonics Inc). was used to collect and analyze left ventricular end-systolic dimensions (LVESD), left ventricular end-diastolic dimensions (LVEDD), and left ventricular internal diastolic diameter (LVIDd). Each rat was measured for 3–6 cardiac cycles, and the average value was calculated. Left ventricular shortening (LVFS) and left ventricular ejection fraction (LVEF) were calculated as follows: LVFS(%) = [(LVEDD-LVESD)/EDD] × 100, LVEF(%) = $[(LVIDd)^3 - (LVIDs)^3]/(LVIDd)^3 \times 100$.

Western Blot Analysis

Protein expression levels were quantified using Western blot analysis. Briefly, the tissue fragments were ground to powder in liquid nitrogen, protein was extracted using (radioimmunoprecipitation assay) RIPA lysis buffer (P0013B, Beyotime Biotechnology) and phosphatase inhibitors (P1005, Beyotime Biotechnology) on ice for 30 min. After repeatly aspirated and thawed the lysates were separated by centrifugation at 12,000 rpm for 10 min at 4°C and the supernatant carefully collected. The concentration in supernatants were detected with Pierce R BCA Protein Assay Kit (23227, Thermo Fisher). Equal amounts of protein lysate were separated by 12% SDS-PAGE and then transferred to PVDF membranes. The membranes were blocked with 5% non-fat dry milk at room temperature for 2 h and incubated overnight at 4◦C with primary antibodies. Subsequently membranes were incubated for 1 h at room temperature with secondary antibodies. The protein bands were exposed with SuperSignal™ West Pico PLUS (34577, Thermo Fisher) and measured by ChemiDoc R XRS+ System (Bio-Rad Laboratories, Hercules, CA, USA). The band density was quantified by Image J software. The following antibodies were used: anti-MMP-8 antibody (1:1000, ab81286) was purchased from Abcam, anti-AKT antibody (1:1000, 9272S), anti-Phospho-Akt (Ser473) antibody (1:1000, 9271S), anti-β-actin antibody (1:1000, 4970T) and HRP-linked anti-rabbit antibody (1:2000, 7074P2) were all purchased from Cell Signaling Technology (Danvers, MA, USA).

Statistical Analysis

All data are presented as mean ± the standard error of the mean (SEM). Unpaired two-tailed Student's t-tests were conducted to compare two groups. SPSS software (version 17.0; IBM Corp., Armonk, NY, USA) was used for the statistical analyses. A one-way analysis of variance with post hoc analysis was used to compare more than two groups. Statistical significance was set at $P < 0.05$.

Results

Characterization of the Mn_3O_4 NZs

As shown in Figure 1A and B, the Mn_3O_4 NZs exhibited a nanoflower-like shape with an average size of 110 nm. The Mn oxidation state was indicated using the XPS spectrum. The high-resolution XPS spectrum of Mn2p showed two main peaks located at 653.6 (Mn2p1/2) and 641.7 eV (Mn2p3/2) with a spin-energy splitting of 11.9 eV (Figure 1C). This spin-energy splitting was performed according to a previous report.[11] Based on the Raman spectroscopy results (Figure 1D), clear characteristic peaks are observed at 654 cm^{-1}, 368 cm^{-1}, and 311 cm^{-1}, with weaker peaks at 471 cm^{-1} and 282 cm^{-1}. The peaks at 654 cm^{-1} and 311 cm^{-1} are attributed to the Mn-O stretching vibrations of Mn^{2+} ions in tetrahedral coordination. The peak at 654 cm^{-1} corresponds to the A1g mode, associated with the Mn-O breathing vibration in the tetrahedral coordination of divalent manganese. The peak at 471 cm^{-1} is ascribed to the Mn^{4+}–O

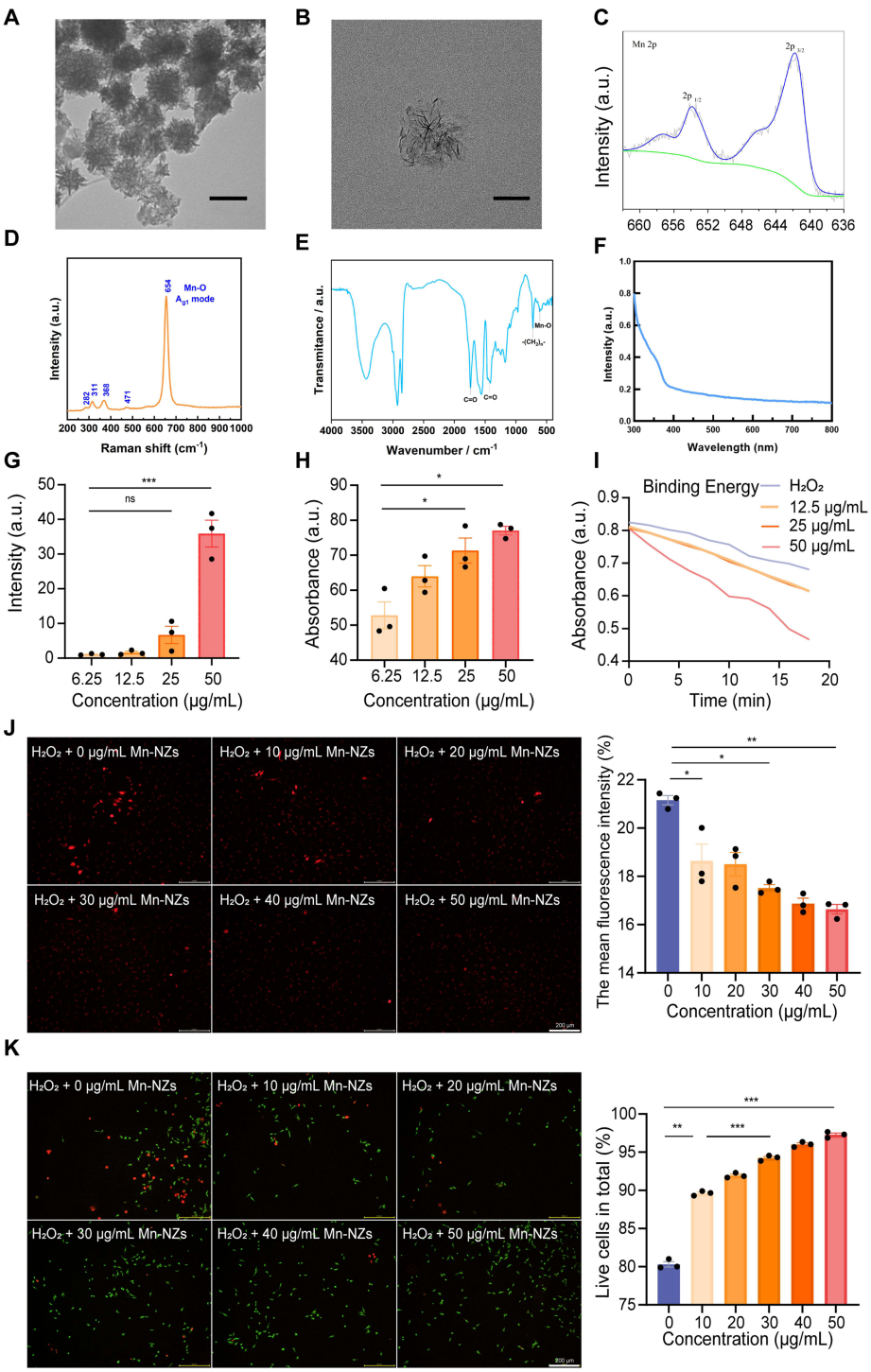

Figure 1 Characterization of Mn_3O_4 NZs. (**A** and **B**) TEM image of Mn_3O_4 NZs, scale bar = 100 nm. (**C**) XPS spectra of Mn_3O_4 NZs. Fitted Mn 2p3/2 and Mn 2p1/2 peaks. (**D**) Raman spectroscopy results of Mn_3O_4 NZs. (**E**) Fourier-transform infrared spectroscopy results of Mn_3O_4 NZs. (**F**) Ultraviolet-visible spectroscopy results of Mn_3O_4 NZs. (**G**) SOD mimetic activity of Mn_3O_4 NZs. (**H**) CAT mimetic activity of Mn_3O_4 NZs. (**I**) GPx mimetic activity of Mn_3O_4 NZs. (**J**) Fluorescence microscope results of ADSCs pre-treated with different concentrations of Mn_3O_4 NZs at 30 μM H_2O_2, scale bar = 200 μm. Statistical analysis of mean fluorescence of ADSCs pre-treated with different concentrations of Mn_3O_4 NZs at 30 μM H_2O_2. (**K**) Fluorescence microscope results of ADSCs pre-treated with different concentrations of Mn_3O_4 NZs at 30 μM H_2O_2, scale bar = 200 μm. Statistical analysis of the percentage of the number of living cells in the total number of ADSCs pre-treated with different concentrations of Mn_3O_4 NZs at 30 μM H_2O_2. *P <0.05, **P < 0.01, ***P < 0.001, ns: no significance.

Abbreviations: NZ, nanozyme; ADSC, adipose-derived stem cell; AMI, acute myocardial infarction; TEM, transmission electron microscopy; XPS, X-ray photoelectron spectroscopy; SOD, superoxide dismutase; CAT, catalase; GPx, glutathione peroxidase.

stretching vibration in an octahedral position. Typically, the characteristic peaks of Mn_3O_4 include a strong peak at 654 cm^{-1} and small peaks at 368 cm^{-1} and 311 cm^{-1}. Additionally, according to the Fourier-transform infrared (FTIR) spectroscopy results (Figure 1E), the absorption peak at 1417 cm^{-1} is assigned to the symmetric stretching vibration mode of carboxylate C=O, indicating coordination between the carboxyl group and manganese ions to form manganese-carboxylate complexes. These complexes act as templates and provide surface stabilization for the subsequent formation of nanoflowers. The absorption peak at 610 cm^{-1} is attributed to the Mn-O stretching vibration in a manganese-oxygen tetrahedral structure, while peaks at 512 cm^{-1} and 420 cm^{-1} correspond to the bending vibrations of Mn-O in a manganese-oxygen octahedral structure. These absorption peaks suggest that at high temperatures, the manganese-carboxylate complexes decompose, leading to the aggregation and reorganization of manganese oxides, which ultimately results in the formation of Mn_3O_4 crystals, confirming the successful synthesis of NZs.

The multi-anti-oxidative enzyme mimetic activities were systematically investigated. The SOD-mimetic catalytic activity of the Mn_3O_4 NZs was measured using the hydroxylamine method. As shown in Figure 1G, the Mn_3O_4 NZs exhibited robust SOD-mimetic catalytic activity in a concentration-dependent manner. Next, the CAT-mimetic activity of the Mn_3O_4 NZs was assessed. The Mn_3O_4 NZs showed enhanced scavenging behavior toward H_2O_2 with increasing Mn_3O_4 NZs concentration. The scavenging rate of H_2O_2 reached about 77% in the presence of 50 μg/mL Mn_3O_4 NZs (Figure 1H). The GPx-mimetic activity of the Mn_3O_4 NZs was evaluated using real-time monitoring of the NADPH absorption at 340 nm. As shown in Figure 1I, the absorption decreased dramatically at a concentration of 50 μg/mL Mn_3O_4 NZs, which indicated that Mn_3O_4 NZs possess ROS scavenging capability via inherent GPx-mimetic catalytic activity.

ADSCs were successfully isolated from the inguinal and axillary adipose tissues of rats and cultured until passages 3–5. Flow cytometric analysis showed that the stem cell surface antigens CD29 and CD90 were positively expressed in ADSCs, whereas CD34, CD45, and the endothelial cell surface antigen CD31 were not expressed (Supplementary results and Figure S1). To verify the role of Mn_3O_4 NZs in enhancing the anti-oxidative effects of ADSCs, we used H_2O_2 to mimic the oxidative stress model in vitro. After pre-treatment with various concentrations of Mn_3O_4 NZs for 1 h, 30 μM H_2O_2 was added to the ADSCs for 2 h. Intracellular ROS levels were detected using DHE assay and standardized using fluorescence intensity. As is shown in Figure 1J, H_2O_2 significantly increased the level of ROS in ADSCs, and Mn_3O_4 NZs pre-treatment attenuated the ROS production in ADSCs under the 30 μM H_2O_2 condition. The ROS fluorescence intensity in the control group was 21.2 ± 0.3 arbitrary units (AU). In the Mn_3O_4 NZs pre-treatment groups, the ROS fluorescence intensities were 19.1 ± 1.3 AU with 10 ng/mL Mn_3O_4 NZs, 19.0 ± 0.3 AU with 20 ng/mL Mn_3O_4 NZs, 17.6 ± 0.2 AU with 30 ng/mL Mn_3O_4 NZs, 17.0 ± 0.4 AU with 40 ng/mL Mn_3O_4 NZs, and 16.8 ± 0.1 AU with 50 ng/mL Mn_3O_4 NZs. This indicated that intracellular ROS were partially cleared after pre-treatment with Mn_3O_4 NZs. To detect the effect of Mn_3O_4 NZs on the survival rate of ADSCs under oxidative stress, live (green) and dead cells (red) were stained after treatment with 30 μM H_2O_2 for 2 h. The average percentage of live cells in the control group was 80.30%, and the percentages in the groups receiving 10, 20, 30, 40, and 50 ng/mL Mn_3O_4 NZs pre-treatment were 89.62%, 91.95%, 94.25%, 96.02%, and 97.29%, respectively (Figure 1K). These results indicated that the survival rate of ADSCs pre-treated with Mn_3O_4 NZs significantly increased under oxidative stress conditions.

In vivo Mn_3O_4 NZ Biocompatibility

The safety of the Mn_3O_4 NZs were evaluated in vivo. Rats were euthanized on day 7 and 14 after Mn_3O_4 NZ injection and blood biochemical parameters were measured, including albumin (ALB), alkaline phosphatase (ALP), serum creatinine (Scr), and total bilirubin (TBL) (Figure 2A). The results indicated no statistical difference between the control and experimental groups. The heart, liver, spleen, lung, and kidney tissues of the rats were subjected to HE staining (Figure 2B). These tissues showed no considerable damage, indicating the biocompatibility of the Mn_3O_4 NZs.

Mn_3O_4 NZs + ADSCs Improves the Prognosis of AMI

ECG revealed that the ejection fraction (EF) and fractional shortening (FS) were significantly higher in the ADSC group than in the PBS group. Additionally, the LVEF and LVFS in the AMI mice treated with Mn_3O_4 NZs + ADSCs were significantly higher than those in either the ADSC or Mn_3O_4 NZs treatment groups (Figure 3A).

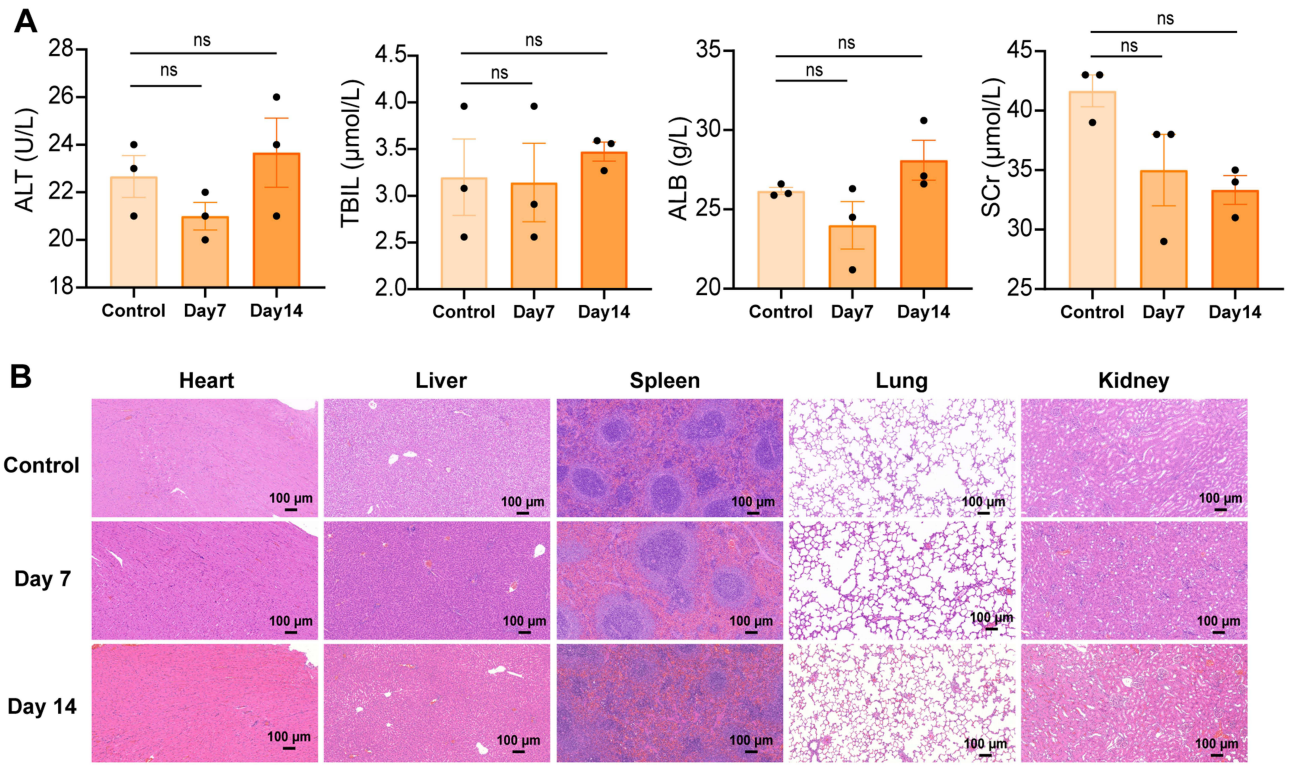

Figure 2 In vivo Mn_3O_4 NZ biocompatibility. (**A**) The results of blood biochemical analysis in rats. (**B**) Hematoxylin and eosin (HE) staining of heart, liver, spleen, lung, and kidney tissues on day 7 and 14 after Mn_3O_4 NZ injection.

The microvascular density in the MI area was significantly higher in the ADSC group than in the PBS group. ADSCs + Mn_3O_4 NZs group further improved the microvascular density in the MI area compared to ADSCs alone (Figure 3B).

The area of cardiac fibrosis in the ADSCs group was significantly less than that of the PBS group, according to Masson trichrome staining (PBS group 54.9 ± 6.0% vs ADSC group 34.5 ± 5.3%). Additionally, compared to the ADSC group, ADSCs + Mn_3O_4 NZs group significantly decreased the infarct size and fibrosis area (ADSCs + Mn_3O_4 NZs group 22.0 ± 3.1% vs ADSCs group 34.5 ± 5.3%). These findings suggest that ADSCs guard against AMI to some extent, and that the combination with Mn_3O_4 NZs can further reduce in vivo AMI damage (Figure 3C).

Mn_3O_4 NZs + ADSCs Can Improve the Survival and Differentiation of ADSCs After Transplantation in AMI Rats

To investigate the potential role of Mn_3O_4 NZs +ADSCs group in the AMI microenvironment, ADSCs were marked with monomeric red fluorescent protein (mRFP). The rats were then subjected to AMI and intramyocardially injected with ADSCs mixed with PBS or 20 ng/mL Mn_3O_4 NZs. The presence of ADSCs in AMI was detected 1 and 4 weeks after ADSC transplantation. At 1 week, the percentage of mRFP-positive cells in the combination group was 17.5 ± 5.3%, while the percentage of mRFP-positive cells in the ADSC group was 10.1 ± 3.0% (Figure 4A). At 4 weeks after transplantation, the percentage of mRFP-positive cells in the combination group was 13.1 ± 4.4%, which was significantly higher than the 6.7 ± 2.5% observed in the ADSC group (Figure 4B). In addition, the cells in the ADSC group were distributed in the area surrounding the MI, but in the ADSCs + Mn_3O_4 NZs group, cells were distributed in both the MI area and the surrounding area. According to the above findings, injecting the Mn_3O_4 NZs + ADSCs combination considerably increased the survival rate of ADSCs at 1 and 4 weeks after transplantation (Figure 4A and B).

Samples were collected 4 weeks after transplantation, and immunofluorescence labeling was performed to detect the ability of ADSCs to differentiate between ADSCs and Mn_3O_4 NZs. The percentage of cardiac troponin T^+/$mRFP^+$ cells was higher in the ADSCs + Mn_3O_4 NZs group than in the ADSCs group (8.6 ± 1.9% vs 4.1 ± 1.7%, Figure 4C). In

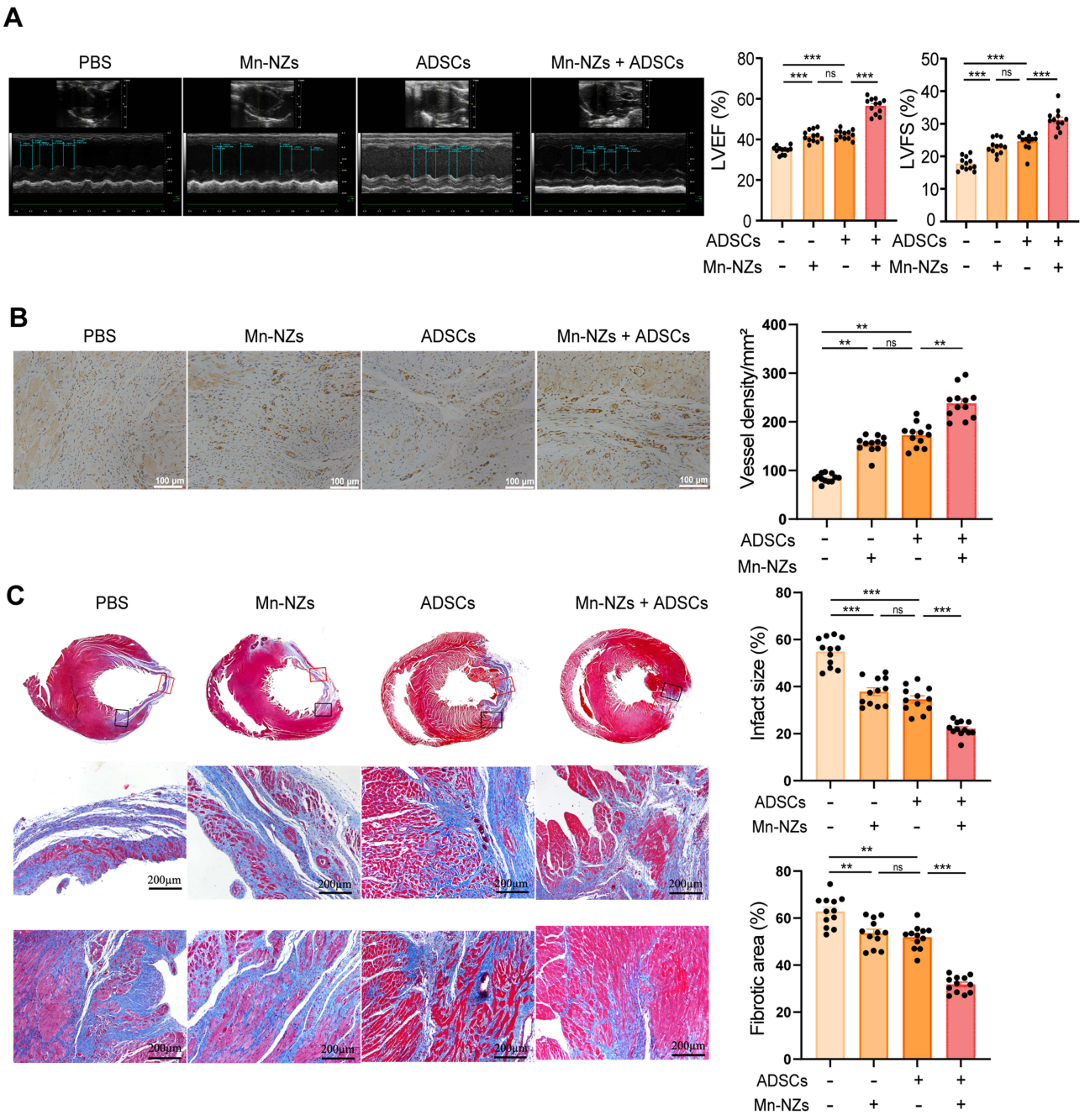

Figure 3 Mn_3O_4 NZs combined with ADSCs improves the prognosis of AMI. (**A**) Representative echocardiographic images of the PBS, Mn_3O_4 NZs alone, ADSCs alone, and Mn_3O_4 NZs + ADSCs combined groups. Statistical analysis results of LVFS and LVEF. (**B**) Representative images of vWF immunohistochemical staining in the PBS, Mn_3O_4 NZs alone, ADSCs alone group, and Mn_3O_4 NZs + ADSCs group, respectively, scale bar = 100 μm. Statistical analysis results of microvascular density. (**C**) Representative images of the Masson staining of the heart section. The general observation photos include the local area viewed with a microscope at high magnification. The red frame shows the area of MI, and the black frame shows the marginal area of MI, scale bar = 200 μm. Statistical analysis results of MI size and collagen deposition. *P <0.05, **P < 0.01, ***P < 0.001, ns: no significance.

Abbreviations: NZs, nanozymes; ADSC, adipose-derived stem cell; AMI, acute myocardial infarction; LVFS, left ventricular shortening score; LVEF, left ventricular ejection fraction; vWF, von Willebrand factor; MI, myocardial infarction; PBS, phosphate-buffered saline.

addition, the coincidence of alpha-smooth muscle actin $(\alpha\text{-SMA})^+/mRFP^+$ cells was also observed in the ADSC injection group and the ADSCs + Mn_3O_4 NZs injection group, suggesting that ADSCs injected into the infarcted myocardium may differentiate into α-SMA-positive vascular smooth muscle cells (Figure 4D).

https://doi.org/10.2147/IJN.S483980

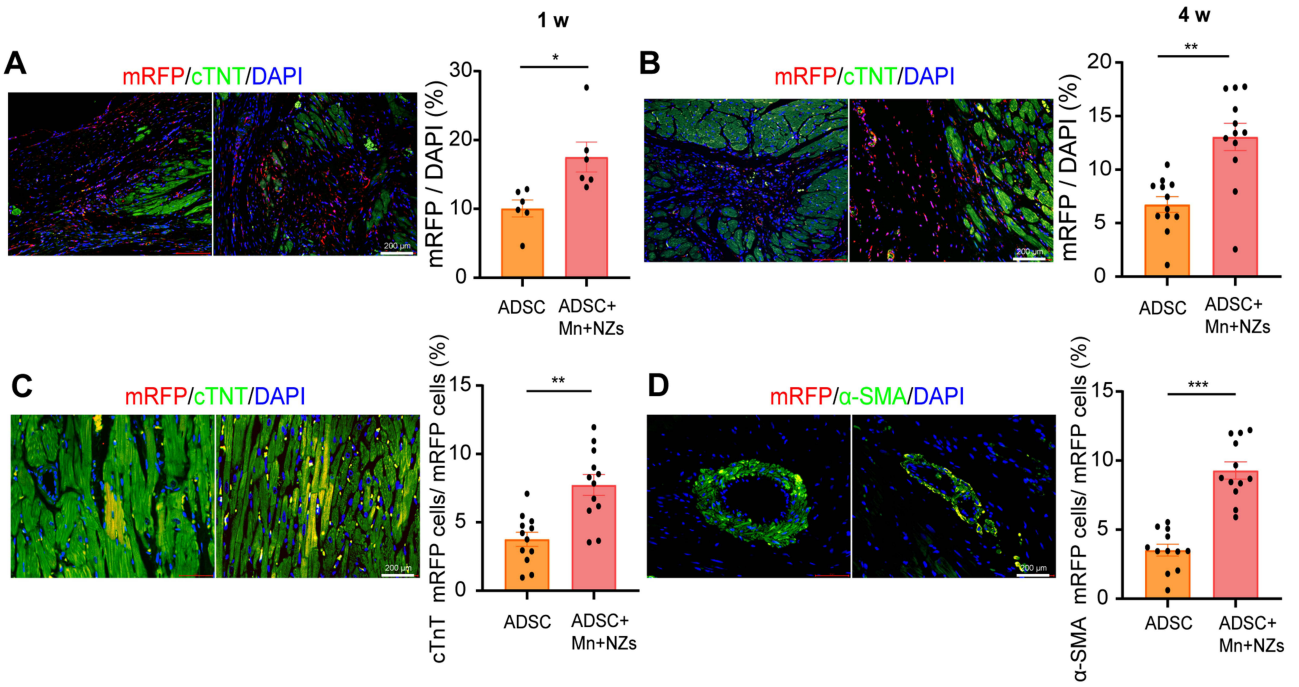

Figure 4 Mn_3O_4 NZs + ADSCs can improve the survival and differentiation of ADSCs after transplantation in AMI rats. (**A**) Fluorescence microscope observation of ADSCs combined with or without Mn_3O_4 NZs at the MI site 1 week after transplantation. Statistical analysis results of the percentage of mRFP -positive ADSCs in DAPI-stained cells 1 week after transplantation. (**B**) Fluorescence microscope observation of ADSCs combined with or without Mn_3O_4 NZs at the MI site 4 weeks after transplantation. Statistical analysis results of the percentage of mRFP-positive ADSCs in DAPI-stained cells 4 weeks after transplantation. (**C**) The cTnT immunofluorescence staining shows representative images of cTnT-positive cardiomyocytes in the ADSCs and Mn_3O_4 NZs + ADSCs injection group, scale bar = 50 μm. Quantitative analysis of myocardial differentiation in the ADSCs and Mn_3O_4 NZs + ADSCs injection groups. (**D**) α-SMA immunofluorescence staining shows representative images of α-SMA-positive vascular smooth muscle cell differentiation in heart sections in the ADSCs and Mn_3O_4 NZs + ADSCs group, scale bar = 30 μm. Quantitative analysis of vascular smooth muscle cell differentiation in the ADSCs and Mn_3O_4 NZs + ADSCs injection groups. *P <0.05, **P < 0.01, ***P < 0.001, ns: no significance.

Abbreviations: NZ, nanozyme; ADSC, adipose-derived stem cell; AMI, acute myocardial infarction; mRFP, monomeric red fluorescent protein; DAPI, 4',6-diamidino-2-phenylindole; α-SMA, alpha-smooth muscle actin; cTnT, cardiac troponin T.

Mn_3O_4 NZs Can Increase the Anti-Oxidant Effect of ADSCs to Improve AMI

To determine the potential signaling pathway responsible for the protective effect of Mn_3O_4 NZs, proteomics was performed. Rats were subjected to AMI and ADSC transplantation with PBS or Mn_3O_4 NZs injection. One week after surgery, the heart samples were harvested for proteomic analysis. Heatmap cluster analysis (Figure 5A) revealed different proteins in the PBS and Mn_3O_4 NZs groups after AMI. The most significant Gene Ontology terms were associated with "complement activation", "fibrinolysis", and "endopeptidase inhibitor activity" (Figure 5B). Kyoto Encyclopedia Genes and Genomes pathway enrichment analysis showed that the "complement and coagulation cascades", and the "staphylococcus aureus infection" were most commonly associated with the protection of the Mn_3O_4 NZs group against AMI injury (Figure 5C). Next, we sought to determine which proteins among the AMI-induced or -suppressed genes were regulated by Mn_3O_4 NZs injection. Differential analysis revealed 66 significantly upregulated and 33 significantly downregulated proteins in AMI-treated with Mn_3O_4 NZs as compared to PBS cells (Figure 5D). Preliminary analysis showed that among the upregulated proteins, some such as Hpx, Map-1, and Mmp8, play an important role in anti-oxidative damage, anti-inflammation, and anti-fibrosis and might participate in the regulation of the microenvironment of AMI.

In previous studies, Hemopexin (Hpx) was an acute phase protein primarily responsible for binding and clearing free hemoglobin from the blood. Map-1, The current researches mainly focused on its function in the nervous system, and there is still a lack of clear evidence to clarify the direct link between Map-1 and acute myocardial infarction. In contrast, there have been numerous research reports on MMP8 in the field of cardiac repairment, providing us with theoretical support for further research. Therefore, we mainly focus on the role and function of MMP8 in the exploration of subsequent mechanisms.

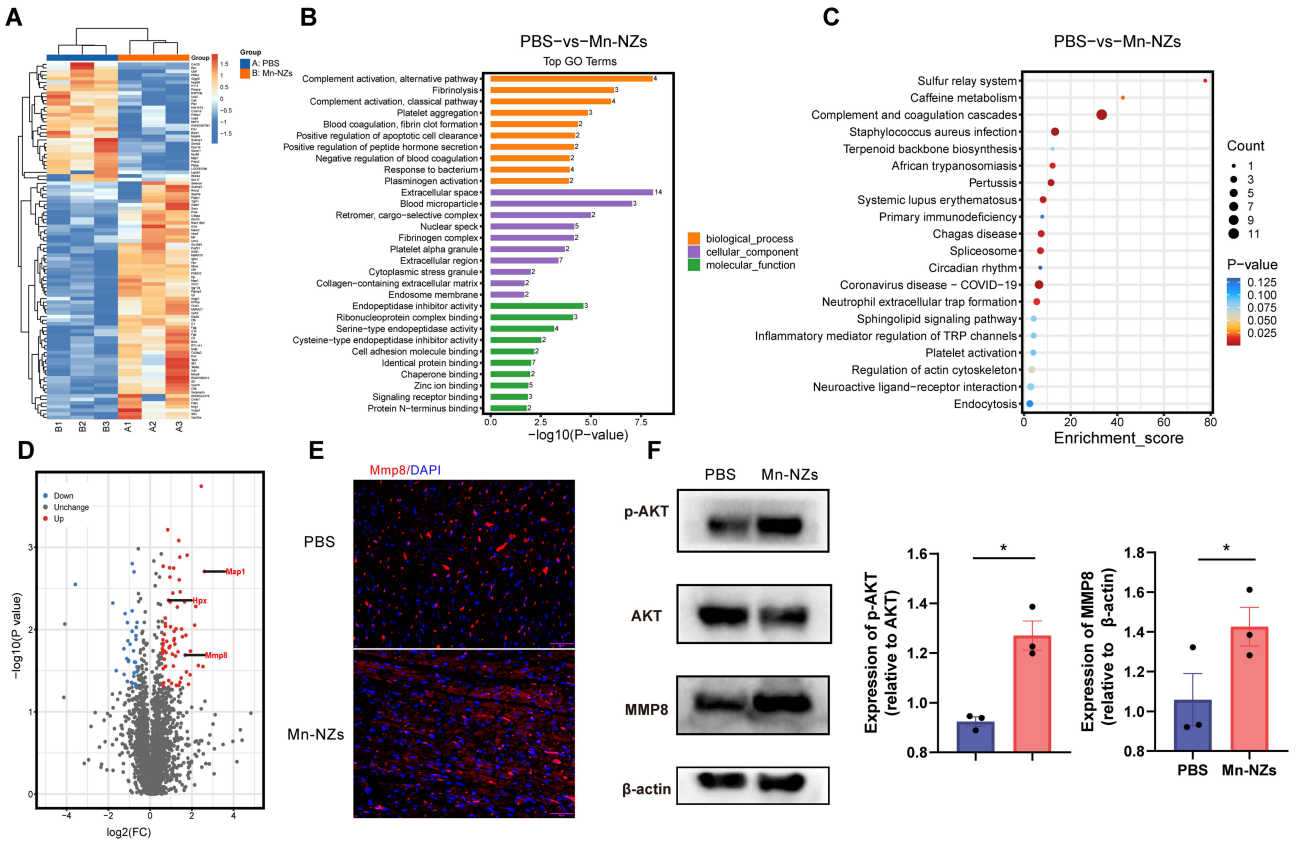

Figure 5 Mn_3O_4 NZs can increase the anti-oxidant effect of ADSCs to improve AMI. (**A**) Heatmap of different proteins in the PBS and Mn_3O_4 NZs groups (n=3). (**B** and **C**) GO and KEGG pathway analysis of different proteins in the PBS and Mn_3O_4 NZs groups. (**C**) Volcano plot of differential genes in PBS and Mn_3O_4 NZs groups. (**E**) The presentation of MMP8 in the MI area. (**F**) Western blots results of MMP8 and related pathway. *P <0.05.

Abbreviations: NZs, nanozymes; ADSC, adipose-derived stem cell; AMI, acute myocardial infarction; PBS, phosphate-buffered saline GO, Gene Ontology; KEGG, Kyoto Encyclopedia of Genes and Genomes.

To verify the proteomic results, we detected the presence of MMP8 in the MI area under a fluorescence microscope a week after transplantation. As shown in Figure 5E, Mn_3O_4 NZs + ADSCs increased the MMP8 levels in the MI area compared to that in the PBS group. To further explore the regulation mechanism of MMP8, Western blot was conducted to determine MMP8 expression and its related pathways. As shown in Figure 5F, p-AKT expression in the treatment group was significantly higher than that in the PBS group, whereas MMP8 expression levels were similar. As such, these results further verified our hypothesis that under Mn-NZ intervention, MMP8 expression was upregulated via AKT pathway phosphorylation.

Discussion

AMI, a leading cause of morbidity and mortality worldwide, often results in irreversible myocardial injury and adverse cardiac remodeling. Therefore, there is an urgent need for innovative therapeutic strategies to mitigate infarction-induced remodeling and improve long-term outcomes in patients with AMI. Over the past decade, regenerative medicine has gained significant attention as a potential treatment for AMI.[21] As a subset of MSCs, ADSCs have emerged as promising candidates for myocardial regeneration due to their ability to differentiate into cardiac cells, secrete paracrine factors that promote angiogenesis and tissue repair, and modulate the immune response in the infarcted heart.[22,23] Mounting evidence suggests that treatment of AMI with ADSCs improves LVEF and decreases the MI area.[24,25] Nevertheless, in the pursuit of heightened efficacy, investigations into combination therapies that comprehensively target the multifarious pathophysiological aspects of AMI are underway. Recently, nanotechnology has opened new avenues for innovative therapeutic strategies. Among the myriad of nanoparticles, Mn_3O_4 NZs have garnered significant attention owing to their unique physicochemical properties. Mn_3O_4 NZs efficiently scavenge ROS, a critical factor in the pathogenesis of AMI-induced

https://doi.org/10.2147/IJN.S483980

oxidative stress and subsequent tissue damage.[17] The combination of ADSC transplantation with Mn_3O_4 NZs offers a multifaceted approach, in which the regenerative potential of ADSCs is complemented by the anti-oxidative and anti-inflammatory properties of Mn_3O_4 NZs, potentially providing a more robust and holistic therapeutic intervention for AMI. In this study, we fabricated Mn_3O_4 NZs and verified their anti-oxidative abilities. The administration of ADSCs improved the prognosis of MI. ADSCs combined with Mn_3O_4 NZs can increase the survival and differentiation of ADSCs in the MI area, further improving cardiac function, reducing fibrosis, and promoting angiogenesis in a rat model of MI. An in vitro H_2O_2 stress model and proteomics analysis demonstrated that Mn_3O_4 NZs enhanced the anti-oxidative effect of ADSCs.

Stem cell transplantation is an effective strategy for promoting tissue regeneration and repairing damaged tissue. The differentiation of MSCs into cardiomyocytes can repair the damaged myocardium and improve cardiac function after MI. In addition, MSCs can produce many factors related to angiogenesis and anti-apoptosis through a paracrine effect to exert cytoprotection on cardiomyocytes.[4] Extensive clinical trials have demonstrated that stem cell therapeutic strategies are feasible and safe for tissue damage repair and functional improvement. However, because of the excessive expression of ROS in the tissue microenvironment, the oxidative stress reaction caused by the accumulation of free radicals leads to myocardial degeneration by inducing lipid peroxidation, protein oxidation, and DNA double-strand breaks, ultimately accelerating the process of cell death in the early stages of AMI.[19] Moreover, the secretion of pro-inflammatory cytokines such as tumor necrosis factor-α, interleukin (IL-1β), and IL-6, and the induction of hypoxia in damaged sites would lead to cell death, ultimately hindering cell proliferation and differentiation.[26] Therefore, the inflammatory and oxidative microenvironment in AMI has adverse effects on cell transplantation, and therefore, it is important to improve the AMI microenvironment to improve the survival rate of transplanted cells, such as ADSCs. Due to adverse microenvironmental effects, such as hypoxia and ischemia of local necrotic tissue at the MI site, and insufficient paracrine signals provided by surrounding healthy myocardial cells, the resident rate, survival rate, and proliferation efficiency of transplanted stem cells are reduced, and the effect of stem cell therapy is not ideal. Interventions to promote differentiation and enhance stem cell cytoprotection may be more reasonable and effective for improving the efficacy of stem cell transplantation. Therefore, a joint strategy based on pre-treatment, regulation of stem cells, and control of their proliferative activity may provide a relevant solution to avoid the death of a large number of donor stem cells after transplantation.

Recently, an increasing number of materials targeting oxidative stress have been used for the treatment of AMI. A novel injectable hydrogel was developed to effectively eliminate ROS and generate O_2.[27] The results showed that the hydrogel not only significantly eliminated excess ROS and inhibited apoptosis but also increased the proportion of M1/M2 macrophages, promoted angiogenesis, reduced infarct size, and significantly improved cardiac function in AMI rats.[28] Therefore, improving the AMI microenvironment while also improving cell function may be an ideal strategy for AMI treatment. In this study, the cardiac function of AMI rats was improved by ADSC injection alone, Mn_3O_4 NZs injection alone, and ADSCs + Mn_3O_4 NZs combination therapy. However, the combination of ADSCs + Mn_3O_4 NZs had the most noticeable effect on cardiac function. Additionally, the simultaneous injection of Mn_3O_4 NZs increased the survival rate and activity of ADSCs in the MI area in rats, enhancing their capacity to provide cardioprotection.

Mechanistically, proteomic analysis has been applied to explore the potential molecules. In our study, Mmp8 was upregulated and confirmed by Western blot and fluorescence microscope. Matrix metalloproteinases (MMPs) are proteolytic enzymes that decompose extracellular matrix (ECM) components. Researches have reported that MMPs play a pivotal role in myocardial remodeling after MI.[29] During the early stage after MI onset, cardiomyocyte necrosis led to activation of MMPs, once activated, MMP-8 could efficiently degrade collagen I, II, and III, which is very important for cardiac repairment after ischemic insults. Studies have exhibited that increased MMP expression is significantly associated with a cardiac remodeling in the human left ventricle of explanted hearts with ischemic dilated cardiomyopathy and in the myocardium with experimental MI,[28] which could explicate the mechanism of combination therapy preliminarily.

Advanced clinical application of nanomaterials depends on their safety after in vivo injection. Mn_3O_4 nanoparticles have been found to be safe and compatible in vivo[30] and further confirmed in our study. We injected Mn_3O_4 NZs (10 mg/kg) at a safe dose and no adverse reactions were observed in the rats in the injection group. Additionally, the combination of Mn_3O_4 NZs + ADSCs increased the residence rate of ADSCs in infarcted areas after AMI surgery. In conclusion, our

study demonstrated that the administration of Mn_3O_4 NZs could enhance the ability of ADSCs to resist the severe AMI microenvironment and eventually help improve the prognosis of MI. Our study provides novel insights into AMI therapy using Mn_3O_4 NZs.

Funding

Nature Science Foundation of Hainan (823QN254, China).

Disclosure

The authors report no conflicts of interest in this work.

References

1. Tsao CW, Aday AW, Almarzooq ZI, et al. Heart disease and stroke statistics-2023 update: a report from the American Heart Association. *Circulation*. 2023;147:e93–e621.
2. Fröhlich GM, Meier P, White SK, Yellon DM, Hausenloy DJ. Myocardial reperfusion injury: looking beyond primary PCI. *Eur Heart J*. 2013;34:1714–1722. doi:10.1093/eurheartj/eht090
3. Amado LC, Saliaris AP, Schuleri KH, et al. Cardiac repair with intramyocardial injection of allogeneic mesenchymal stem cells after myocardial infarction. *Proc Natl Acad Sci U S A*. 2005;102:11474–11479. doi:10.1073/pnas.0504388102
4. Shake JG, Gruber PJ, Baumgartner WA, et al. Mesenchymal stem cell implantation in a swine myocardial infarct model: engraftment and functional effects. *Ann Thorac Surg*. 2002;73:1919–1925, 1926. doi:10.1016/S0003-4975(02)03517-8
5. Monguió-Tortajada M, Prat-Vidal C, Martínez-Falguera D, et al. Acellular cardiac scaffolds enriched with MSC-derived extracellular vesicles limit ventricular remodelling and exert local and systemic immunomodulation in a myocardial infarction porcine model. *Theranostics*. 2022;12:4656–4670. doi:10.7150/thno.72289
6. Chiu TL, Baskaran R, Tsai ST, et al. Intracerebral transplantation of autologous adipose-derived stem cells for chronic ischemic stroke: a phase I study. *J Tissue Eng Regen M*. 2022;16:3–13. doi:10.1002/term.3256
7. Wang W, Tan B, Chen J, et al. An injectable conductive hydrogel encapsulating plasmid DNA-eNOs and ADSCs for treating myocardial infarction. *Biomaterials*. 2018;160:69–81. doi:10.1016/j.biomaterials.2018.01.021
8. Yuan Z, C C, Qin Y, et al. CXCR4(+) sorted adipose-derived stem cells enhance their functional benefits and improve cardiac function after myocardial infarction[J]. *Stem Cells Int*. 2022;2022:6714765. doi:10.1155/2022/6714765
9. Yang S, Sun Y, Yan C. Recent advances in the use of extracellular vesicles from adipose-derived stem cells for regenerative medical therapeutics[J]. *J Nanobiotechnol*. 2024;22(1):316. doi:10.1186/s12951-024-02603-4
10. Yoshizaki Y, Takai H, Mayumi N, et al. Cellular therapy for myocardial ischemia using a temperature-responsive biodegradable injectable polymer system with adipose-derived stem cells[J]. *Sci Technol Adv Mater*. 2021;22(1):627–642. doi:10.1080/14686996.2021.1938212
11. Kawamura T, Yoshioka D, Kawamura A, et al. Safety and therapeutic potential of allogeneic adipose-derived stem cell spray transplantation in ischemic cardiomyopathy: a phase I clinical trial[J]. *J Transl Med*. 2024;22(1):1091. doi:10.1186/s12967-024-05816-1
12. Singh N, Sherin GR, Mugesh G. Antioxidant and prooxidant nanozymes: from cellular redox regulation to next-generation therapeutics. *Angew Chem Int Ed Engl*. 2023;62:e202301232. doi:10.1002/anie.202301232
13. Singh N, Savanur MA, Srivastava S, D'Silva P, Mugesh G. A manganese oxide nanozyme prevents the oxidative damage of biomolecules without affecting the endogenous antioxidant system. *Nanoscale*. 2019;11:3855–3863. doi:10.1039/C8NR09397K
14. Hansch R, Mendel RR. Physiological functions of mineral micronutrients (Cu, Zn, Mn, Fe, Ni, Mo, B, Cl). *Curr Opin Plant Biol*. 2009;12:259–266. doi:10.1016/j.pbi.2009.05.006
15. Singh N, Savanur MA, Srivastava S, D'Silva P, Mugesh G. A redox modulatory Mn3 O4 nanozyme with multi-enzyme activity provides efficient cytoprotection to human cells in a Parkinson's disease model. *Angew Chem Int Ed*. 2017;56:14267–14271. doi:10.1002/anie.201708573
16. Yao J, Cheng Y, Zhou M, et al. ROS scavenging Mn(3)O(4) nanozymes for in vivo anti-inflammation. *Chem Sci*. 2018;9:2927–2933. doi:10.1039/C7SC05476A
17. Li L, Xiao B, Mu J, et al. A MnO2 nanoparticle-dotted hydrogel promotes spinal cord repair via regulating reactive oxygen species microenvironment and synergizing with mesenchymal stem cells. *ACS Nano*. 2019;13:14283–14293. doi:10.1021/acsnano.9b07598
18. Zhang B, Chen G, Wu X, et al. Biomimetic Prussian blue nanozymes with enhanced bone marrow-targeting for treatment of radiation-induced hematopoietic injury. *Biomaterials*. 2023;293:121980. doi:10.1016/j.biomaterials.2022.121980
19. Chen G, Deng H, Song X, et al. Reactive oxygen species-responsive polymeric nanoparticles for alleviating sepsis-induced acute liver injury in mice. *Biomaterials*. 2017;144:30–41. doi:10.1016/j.biomaterials.2017.08.008
20. Yang C, Tibbitt MW, Basta L, Anseth KS. Mechanical memory and dosing influence stem cell fate. *Nat Mater*. 2014;13:645–652. doi:10.1038/nmat3889
21. Abdolmohammadi K, Mahmoudi T, Alimohammadi M, Tahmasebi S, Zavvar M, Hashemi SM. Mesenchymal stem cell-based therapy as a new therapeutic approach for acute inflammation. *Life Sci*. 2023;312:121206. doi:10.1016/j.lfs.2022.121206
22. Zhang Y, Yang N, Huang X, et al. Melatonin engineered adipose-derived biomimetic nanovesicles regulate mitochondrial functions and promote myocardial repair in myocardial infarction. *Front Cardiovas Me*. 2022;9: 789203.
23. Wang T, Li T, Niu X, et al. ADSC-derived exosomes attenuate myocardial infarction injury by promoting miR-205-mediated cardiac angiogenesis. *Biol Direct*. 2023;18. doi:10.1186/s13062-023-00361-1
24. Yan W, Chen Y, Guo Y, et al. Irisin promotes cardiac homing of intravenously delivered MSCs and protects against ischemic heart injury. *Adv Sci*. 2022;9. doi:10.1002/advs.202103697
25. Long G, Wang Q, Li S, et al. Engineering of injectable hydrogels associate with Adipose-Derived stem cells delivery for anti-cardiac hypertrophy agents. *Drug Deliv*. 2021;28:1334–1341. doi:10.1080/10717544.2021.1943060

26. Khodayari S, Khodayari H, Amiri AZ, et al. Inflammatory microenvironment of acute myocardial infarction prevents regeneration of heart with stem cells therapy. *Cell Physiol Biochem*. 2019;53:887–909. doi:10.33594/000000180
27. Ding J, Yao Y, Li J, et al. A reactive oxygen species scavenging and O2 generating injectable hydrogel for myocardial infarction treatment in vivo. *Small*. 2020;16. doi:10.1002/smll.202005038
28. López E, Blázquez R, Marinaro F, et al. The intrapericardial delivery of extracellular vesicles from cardiosphere-derived cells stimulates M2 polarization during the acute phase of porcine myocardial infarction. *Stem Cell Rev Rep*. 2020;16:612–625. doi:10.1007/s12015-019-09926-y
29. Ding J, Yao Y, Li J, et al. A Reactive oxygen species scavenging and O (2) generating injectable hydrogel for myocardial infarction treatment in vivo[J]. *Small*. 2020;16(48):e2005038.
30. Zhan Y, Shi S, Ehlerding EB, et al. Antibody-conjugated manganese oxide nanoparticles for tumor vasculature targeted positron emission tomography and magnetic resonance imaging. *ACS Appl Mater Inter*. 2017;9:38304–38312. doi:10.1021/acsami.7b12216